



Global Biogeochemical Cycles^a

RESEARCH ARTICLE

10.1029/2023GB008029

Anh Le-Duy Pham and Pierre Damien contributed equally to this work.

Key Points:

- Shelf-to-basin transport is a major source of iron to the North East Pacific
 Ocean
- Half of this transport occurs year-round by downslope Ekman flow in the bottom boundary layer, sustained by the poleward California Undercurrent
- Regional hot-spots of iron transport are sustained by meanders in the poleward undercurrent and local bottom oxygen depletion

Supporting Information:

Supporting Information may be found in the online version of this article.

Correspondence to:

A. L.-D. Pham and P. Damien, anhlpham78@ucla.edu; pdamien@g.ucla.edu

Citation:

Pham, A. L.-D., Damien, P., McCoy, D., Mar, M., Kessouri, F., McWilliams, J. C., et al. (2024). The shelf-to-basin transport of iron from the northern U.S. West Coast to the Pacific Ocean. *Global Biogeochemical Cycles*, 38, e2023GB008029. https://doi.org/10.1029/2033GB008029

Received 6 NOV 2023 Accepted 14 APR 2024

The Shelf-To-Basin Transport of Iron From the Northern U. S. West Coast to the Pacific Ocean

Anh Le-Duy Pham¹, Pierre Damien¹, Daniel McCoy¹, Matthew Mar¹, Fayçal Kessouri², James C. McWilliams¹, James Moffett³, and Daniele Bianchi¹

¹Department of Atmospheric and Oceanic Sciences, University of California Los Angeles, Los Angeles, CA, USA, ²Southern California Coastal Water Research Project, Costa Mesa, CA, USA, ³Department of Biological Sciences, University of Southern California, Los Angeles, CA, USA

Abstract Release of iron (Fe) from continental shelves is a major source of this limiting nutrient for phytoplankton in the open ocean, including productive Eastern Boundary Upwelling Systems. The mechanisms governing the transport and fate of Fe along continental margins remain poorly understood, reflecting interaction of physical and biogeochemical processes that are crudely represented by global ocean biogeochemical models. Here, we use a submesoscale-permitting physical-biogeochemical model to investigate processes governing the delivery of shelf-derived Fe to the open ocean along the northern U.S. West Coast. We find that a significant fraction (~20%) of the Fe released by sediments on the shelf is transported offshore, fertilizing the broader Northeast Pacific Ocean. This transport is governed by two main pathways that reflect interaction between the wind-driven ocean circulation and Fe release by low-oxygen sediments: the first in the surface boundary layer during upwelling events; the second in the bottom boundary layer, associated with pervasive interactions of the poleward California Undercurrent with bottom topography. In the water column interior, transient and standing eddies strengthen offshore transport, counteracting the onshore pull of the mean upwelling circulation. Several hot-spots of intense Fe delivery to the open ocean are maintained by standing meanders in the mean current and enhanced by transient eddies and seasonal oxygen depletion. Our results highlight the importance of fine-scale dynamics for the transport of Fe and shelf-derived elements from continental margins to the open ocean, and the need to improve representation of these processes in biogeochemical models used for climate studies.

Plain Language Summary Iron is an essential nutrient that supports the life of marine organisms. In the ocean, large quantities of iron are released by sediments found along the continents. However, this iron is not very soluble, and it tends to precipitate back to the sediments close to where it is released. In fact, we still struggle to understand how enough of this iron makes its way to the open ocean, where it fertilizes phytoplankton and sustains fisheries. In this study, we use a sophisticated computer simulation of the ocean currents and chemistry of the northern U.S. West Coast to study the transport of iron released along the continent to the open ocean. This computer simulation is able to reproduce the currents observed along the coast with high realism, including small swirls, eddies, and meanders that constantly mix coastal waters with open ocean waters. We found that about one-fifth of all the iron released by sediments along the coast is transported offshore, where it can sustain the life of marine organisms. This transport from the coast to the open ocean mostly takes place near the surface, reflecting upwelling caused by winds in the summer, and near the bottom, reflecting transport caused by the friction of the poleward California Undercurrent with the seafloor. We also found that episodic swirls, eddies, and meanders reinforce this delivery of iron to the open ocean, in particular along several "hotspots" of intense transport along the coast. Our results suggest that global computer simulations used to study how marine ecosystems respond to climate change should improve how they represent small-scale currents and their effects on the cycle of iron, in particular along the ocean's coastlines.

1. Introduction

The micronutrient iron (Fe) limits primary production in about half of the world's oceans, regulating past and future changes in marine ecosystems and the global carbon cycle (Boyd & Ellwood, 2010; C. M. Moore et al., 2013; Tagliabue et al., 2017). The mechanisms controlling the oceanic Fe cycle have been studied extensively. However, because of complex interactions between external sources and internal cycling processes

© 2024. American Geophysical Union. All Rights Reserved.

PHAM ET AL. 1 of 19

that are still poorly constrained, our ability to model the Fe cycle remains limited, hindering projections of future oceanic productivity and ecosystem change (Tagliabue et al., 2016, 2017).

Major sources of Fe in the ocean include atmospheric deposition (Duce & Tindale, 1991; Jickells et al., 2005), benthic release from continental shelves (Elrod et al., 2004; Johnson et al., 1999), hydrothermal vents (Fitzsimmons et al., 2014; Resing et al., 2015; Tagliabue et al., 2010), sea-ice melting (Person et al., 2021), and river runoffs (Krachler & Krachler, 2021; Vieira et al., 2020). Once in the ocean, Fe exists mostly as the poorly soluble ferric Fe, which quickly precipitates or is rapidly scavenged onto marine particles (Honeyman et al., 1988; X. Liu & Millero, 2002; Tagliabue et al., 2019). Fe can be protected from removal by forming complexes with organic ligands produced by a myriad of biological processes (Buck et al., 2010; Moffett & Boiteau, 2024; van den Berg, 1995). Fe sources, sinks, and protection mechanisms are not fully understood and constrained by in situ measurements and ocean biogeochemical models (Tagliabue et al., 2016, 2017).

Among major sources of Fe to the ocean, the release from continental shelves and slope sediments has received particular attention (Dinniman et al., 2020; Elrod et al., 2004; Johnson et al., 1999; St-Laurent et al., 2017, 2019), especially in Eastern Boundary Upwelling System (EBUS), where Fe often limits primary production (Biller et al., 2013; Hogle et al., 2018; Messié & Chavez, 2015; Till et al., 2019) despite significant benthic fluxes (Dale et al., 2015; Elrod et al., 2004; Severmann et al., 2010). In EBUS, low concentrations of dissolved oxygen (O_2) in bottom waters and high rates of organic matter deposition enhance Fe release from the sediments (Conway & John, 2014; Dale et al., 2015; Lam et al., 2020; Severmann et al., 2010). Benthic Fe sources can exceed Fe delivery by atmospheric deposition and rivers (Deutsch et al., 2021; Robinson et al., 2022), supporting the high primary production observed in EBUS (Elrod et al., 2004; Johnson et al., 1999; Messié & Chavez, 2015). Benthic Fe that escapes phytoplankton uptake and scavenging on the shelf can be transported to the open ocean by subsurface currents (Siedlecki et al., 2012). In the presence of upwelling and vertical mixing, this Fe can fertilize phytoplankton in remote ocean regions, linking the cycles of carbon, O_2 , and Fe (Johnson et al., 1999; Rapp et al., 2020; Wallmann et al., 2022).

Despite intense release from EBUS margins, it is unclear how much Fe reaches the open ocean (Lam et al., 2020; Scholz et al., 2016). Global modeling studies suggest that most benthic Fe is quickly removed by scavenging close to where it is released, restricting its impact to coastal waters (J. K. Moore & Braucher, 2008; J. K. Moore et al., 2004). In contrast, in situ measurements and satellite observations indicate that Fe originating from continental margins can influence primary production hundreds to thousands of kilometers offshore (Elrod et al., 2004; Lam et al., 2006; J. K. Moore & Abbott, 2000).

The export of sediment-derived Fe to the open ocean, here referred to as the shelf-to-basin transport, occurs by a variety of physical processes, including upwelling and vertical mixing, Ekman transport in the surface and bottom boundary layers (SBL and BBL respectively), and eddies (Conway et al., 2018; Fiechter & Moore, 2012; Keith Johnson et al., 2005; Lam et al., 2020; Tagliabue, Sallee, et al., 2014). These circulation patterns are not adequately represented in global ocean Fe models (Tagliabue et al., 2016) because of their coarse resolution, which limits their ability to capture fine scale currents in the regions where most benthic Fe release and transport occur. These include shallow and narrow shelves, where submesoscale processes dominate (Dauhajre et al., 2017; McWilliams, 2016), but also the transition between continental margins and the open-ocean. In this region, transport reflects mesoscale processes such as meanders in the prevailing currents, eddies, and zonal jets (Conway et al., 2018; Cravatte et al., 2017; Uchida et al., 2020), and finer-scale currents, such as submesoscale coherent vortices(McWilliams, 1985). These subsurface coherent eddies are pervasive along EBUS (McCoy et al., 2020), including the California Current System (Pelland et al., 2013), where they form by instability of the poleward Undercurrent (Molemaker et al., 2015) and cause offshore transport of biogeochemical tracers (Frenger et al., 2018). By trapping BBL waters, subsurface coherent eddies likely provide an efficient Fe delivery pathway from continental margins to the ocean interior. Given the importance of mesoscale and submesoscale currents, the role of the shelf-to-basin transport is likely underestimated in current global biogeochemical models.

The seminal study by Siedlecki et al. (2012) provided an expanded picture of the processes that ultimately deliver Fe to the open ocean in EBUS. By using an idealized numerical model of the California Current, they showed that, on average, Fe accumulating in the BBL during upwelling periods is transported to the ocean interior when wind reverses to downwelling-favorable conditions. During wind reversals, thickening of BBL waters, favored by intense vertical shear, generates a Fe-rich plume that detaches from the upper continental slope and delivers Fe to the open ocean via isopycnal transport. The study indicated that, depending on the frequency of wind reversals,

PHAM ET AL. 2 of 19

between 10% and 50% of sediment-derived Fe could be delivered offshore, with the remaining part primarily consumed on the shelf by biological activity. A stronger and shallower poleward Undercurrent would further increase the fraction of Fe exported off the shelf. However, the study was idealized in nature, and not designed to reproduce realistic Fe concentrations and their long-term distribution under competing physical-biogeochemical dynamics.

Here, we build on this work to examine the fate of benthic Fe in a realistic, submesoscale permitting simulation of the U.S. West Coast circulation and biogeochemistry (Damien et al., 2023; Kessouri et al., 2020). We use the model to elucidate the seasonal balances behind the shelf-to-basin Fe transport and its variability along the Northeast Pacific continental margin, with particular focus on interactions between sedimentary Fe release and bottom O_2 and the frictional dynamics of the California Undercurrent under realistic topography, wind, and fine-scale circulation patterns. While we focus on the well-studied California Current system, our findings shed light on dynamics that are likely to occur in other EBUS and, more broadly, along continental shelves and slopes, with the potential to inform global models of Fe and other trace elements (Conway et al., 2018; Jersild et al., 2021; St-Laurent et al., 2017).

The rest of the paper is organized as follows. In Section 2, we describe the model configuration, Fe budget analysis, and framework to identify Fe transport processes and contribution of eddies. In Section 3, we evaluate the model against observations and discuss the Fe balance and transport rates along the northern U.S. West Coast. In Section 4, we discuss the implications of these results for the global Fe cycle and conclude the paper.

2. Methods

2.1. The Regional Oceanic Modeling System (ROMS)

We use a well-established physical-biogeochemical model of the California Current system (Damien et al., 2023; Deutsch et al., 2021; Renault et al., 2021). The physical component consists of the Regional Ocean Modeling System, ROMS (Shchepetkin, 2015; Shchepetkin & McWilliams, 2005), a primitive-equation, hydrostatic, topography-following (i.e., σ coordinate) ocean model. We focus on a northern U.S. West Coast configuration extending from 36.8° N to 49.8° N and 112.5° W to 144.7° W. The grid is composed of $630 \times 1,340$ cells with a horizontal resolution of approximately 1 km and 60 terrain-following vertical levels (Damien et al., 2023). This horizontal grid spacing resolves the narrow topography of the shelf in this region, which rarely exceeds a width of 20 km. The model grid is stretched in the vertical to provide higher resolution near the surface and the seafloor, and better capture boundary layer dynamics. On the shelf (depth shallower than 200 m), the vertical grid includes at least 13 grid points in the upper 25 m of the water column and 6 in the deeper 25 m. The high resolution is essential to resolve mesoscale and submesoscale variability (Capet et al., 2008; Kessouri et al., 2020), the intensified wind-driven overturning circulation on the continental shelf (Damien et al., 2023), and the resulting cross-shore exchange of nutrients and Fe. The model is run for the 1997-2017 period, using a time step of 150 s, and initial and boundary conditions from a "parent" configuration at 4 km resolution (Deutsch et al., 2021). The numerical setup does not include tidal forcings. Model output is saved as daily averages for tracers and monthly averages for physical and biogeochemical fluxes. A detailed discussion of the model configuration, setup, forcings, and initialization is presented in previous publications (Damien et al., 2023; Deutsch et al., 2021; Kessouri et al., 2020; Renault et al., 2021).

2.2. The Biogeochemical Elemental Cycling (BEC) Ecosystem Model

ROMS is coupled online to the Biogeochemical Elemental Cycling model, BEC (J. K. Moore & Braucher, 2008; J. K. Moore et al., 2004). BEC represents the cycles of nutrients (including Fe), O_2 , carbon, alkalinity, and organic matter as driven by three phytoplankton and one zooplankton functional groups (Deutsch et al., 2021; J. K. Moore & Braucher, 2008; J. K. Moore et al., 2004). Remineralization of sinking organic matter is parameterized according to the mineral ballast model of Armstrong et al. (2001). Air-sea fluxes of O_2 and carbon dioxide are based on the gas-exchange model of Wanninkhof (1992).

The Fe cycle in BEC includes four separate pools: dissolved inorganic Fe (dFe), Fe scavenged onto sinking particles, including lithogenic minerals from dust deposition, and Fe associated with organic matter pools. Only the dFe and organically bound Fe pools are modeled as state variables (J. K. Moore & Braucher, 2008; J. K. Moore et al., 2004). For the dFe pool, four processes are considered: atmospheric deposition, biological uptake

PHAM ET AL. 3 of 19

and remineralization, scavenging by sinking particles, and release by sediments. Atmospheric Fe deposition is based on the dust climatology of Mahowald et al. (2005). The model does not include river sources for Fe, except through the Juan De Fuca Strait. While prior work suggests that benthic sources dominate Fe inputs coast-wide, rivers are locally important sources of Fe in the northern California Current. Thus, the lack of river inputs of Fe in the model could lead to biases in the spatial and temporal variability of modeled Fe distribution (Chase et al., 2007; Severmann et al., 2010; Wetz et al., 2006).

Release of Fe from the sediment follows the O_2 -dependent parameterization by Deutsch et al. (2021), obtained by a fit to a compilation of benthic flux chamber measurements in the California margin (Severmann et al., 2010):

$$\log_{10}\Phi(Fe) = 2.5 - 0.0165 \cdot O_2,\tag{1}$$

where O_2 is in mmol m⁻³ and the benthic Fe flux $\Phi(Fe)$ in μ mol m⁻² d⁻¹ (Deutsch et al., 2021). We find this parameterization adequate to capture the observed range of benthic Fe fluxes and their seasonal and alongshore variability (Severmann et al., 2010).

Additional details on the BEC configuration, forcings, coupling with ROMS, and validation of the model solution are presented in Deutsch et al. (2021). A discussion of the wind-driven shelf circulation and biogeochemistry is presented in Damien et al. (2023). In the following, we further evaluate the solution against available measurements of dissolved Fe concentrations along the northern U.S. West Coast (Section 2.3).

2.3. Dissolved Fe Measurements Along the Northern U.S. West Coast

We compiled a data set of dFe measurements from Baja California to Vancouver Island from 23 published studies between 1987 and 2022, resulting in approximately 4,068 individual dFe measurements (Bundy, Jiang, et al., 2016; Hogle et al., 2018; Johnson et al., 2003; King & Barbeau, 2011). A list of the studies and references is presented in Table S1 of the Supporting Information S1. These include a global compilation (Tagliabue et al., 2016), cruises from regional observational programs (Bundy, Jiang, et al., 2016; Hogle et al., 2018; Johnson et al., 2003; King & Barbeau, 2007), and independent studies (Biller & Bruland, 2013; Boiteau et al., 2019; Bundy et al., 2014, 2015; Chappell et al., 2019; Chase et al., 2002, 2005; Firme et al., 2003; Hawco et al., 2021; John et al., 2012; Till et al., 2019).

For this compilation, we define dFe as the sum of both the truly dissolved Fe and the dissolvable Fe, based on the definitions used in the original references. Different studies used varying filter sizes to characterize the dissolved and dissolvable Fe pools, with 0.2, 0.4, and 0.45 μ m as the most common. Measurement methods also vary between studies. In general, measurements were taken with bottles, pump system, and/or by surface tows. In some cases, samples were acidified for short periods of time before analysis. Despite variability in sampling approaches, we find a good agreement between different sets of observations and consider the merged data set as representative of the dFe distribution in the California Current. The final compilation includes observations from 1980 to 2021, with most of the data between 1997 and 2015 and in the upper 100 m of the water column.

2.4. Model Analysis and Diagnostics

2.4.1. Dissolved Fe Budget Analysis

To investigate the fate of the shelf-derived Fe, we analyze the balance between transport fluxes and biogeochemical sources and sinks based on the model conservation equation for dFe, that is, the model dFe budget. We use output from a 9-year period from 2008 to 2016, spanning the region from Cape Mendocino to Vancouver Island. We focus on this region because it encompasses the Washington and Oregon continental shelves, where strong bottom water hypoxia occurs, leading to high benthic Fe release fluxes from low- O_2 sediments. The dFe budget includes external sources from atmospheric deposition and benthic inputs, biological cycling processes consisting of uptake by phytoplankton and remineralization and recycling, scavenging and burial in the sediment, and physical transport by currents and vertical mixing. We calculate biogeochemical rates and physical fluxes online in the model at each time step and average them in time to construct monthly climatologies. The budget of all tracers is closed to numerical precision and scaled up from individual grid cells to three-dimensional regions by numerical integration.

PHAM ET AL. 4 of 19

2.4.2. Eddy Decomposition of the Shelf-To-Basin Fe Transport

We define the shelf-to-basin transport as the advective flux of dissolved Fe across a vertical surface that intersects the 200 m depth isobath, here taken as the boundary between the shelf and the open ocean (Laruelle et al., 2013), using the approach by Damien et al. (2023), which naturally incorporates variations in the topography of the western U.S. coastline. Accordingly, Fe transport is calculated as:

$$T = u \cdot Fe, \tag{2}$$

where Fe is the dFe concentration, and u the cross-shelf horizontal current.

To elucidate the mechanisms responsible for the delivery of Fe from the shelf to the open ocean, we decompose the cross-shelf Fe transport *T* into contributions from the large-scale mean cross-shelf current, standing eddies and meanders, and transient eddies. The large-scale mean transport includes seasonal upwelling and Ekman transport in the SBL and BBL that occur broadly along the coast. Standing eddies and meanders represent circulation patterns that are relatively persistent in time but cause meridional variability along the coast and support localized hot-spots of shelf-to-basin exchange. (Here, we use the terms "standing eddies" and "standing meanders" interchangeably to refer to persistent circulation features embedded within the main alongshore currents that lead to cross-shelf transport.) In contrast, transient eddies represent the contribution of time-varying flow driven by high-frequency fluctuations in winds and instabilities in the mesoscale and submesoscale circulation.

We quantify these components by following the transport decomposition by Lee and Coward (2003). This approach involves two low-pass filters, one in time and one in space. Accordingly, an arbitrary model variable X can be decomposed into time mean and fluctuating components as:

$$X = \overline{X} + X',\tag{3}$$

where $\overline{X} = \frac{1}{\tau} J_{t-\frac{\tau}{2}}^{t+\frac{\tau}{2}} X dt$, with $\tau = 1$ month. Here, \overline{X} is the monthly climatological mean of the variable and $X' = X - \overline{X}$ is the transient eddy fluctuations on time scales shorter than a month.

Similarly, X can be decomposed into an alongshore mean plus a spatial variation around this mean as:

$$X = [X] + X^*, \tag{4}$$

where $[X] = \frac{1}{L} \int_0^L X \, dL$, with L is the length of the shelf along the U.S. West Coast. Here, [X] is the alongshore mean of the variable along the 200 m isobath and $X^* = X - [X]$ is the alongshore fluctuations.

By applying the spatial and temporal filters to the cross-shelf Fe flux, $T = u \cdot Fe$, the mean Fe transport across the shelf break can be expressed as:

$$\left[\overline{T}\right] = \left[\overline{u}\,\overline{Fe}\right] = \left[\overline{u}\right]\left[\overline{Fe}\right] + \left[\overline{u}^*\overline{Fe}^*\right] + \left[\overline{u'}\left\|\overline{Fe'}\right\| + \left[\overline{u'^*Fe'^*}\right],\tag{5}$$

where the full derivation is shown in Appendix A. We further set:

$$\left[\overline{T^{MM}}\right] = \left[\overline{u}\right]\left[\overline{Fe}\right],\tag{6}$$

$$\left[\overline{T^{\text{SE}}}\right] = \left[\overline{u}^* \overline{Fe}^*\right],\tag{7}$$

$$\left[\overline{T^{TE}}\right] = \left[\overline{u'}\right]\left[Fe'\right] + \left[\overline{u'^*Fe'^*}\right] = \left[\overline{u'Fe'}\right]. \tag{8}$$

Here, $\left[\overline{T^{MM}}\right]$ is the cross-shelf Fe transport driven by the climatological mean circulation and Fe distribution, $\left[\overline{T^{\text{SE}}}\right]$ is the cross-shelf transport driven by standing eddies and meanders that cross the shelf break, and $\left[\overline{T^{TE}}\right]$ is

PHAM ET AL. 5 of 19

19449224, 2024, 5, Downloaded from https://agupubs.onlinelibrary.wiley.com/doi/10.1029/2023GB008029 by University Of California, Los, Wiley Online Library on [08/05/2024]. See the Term

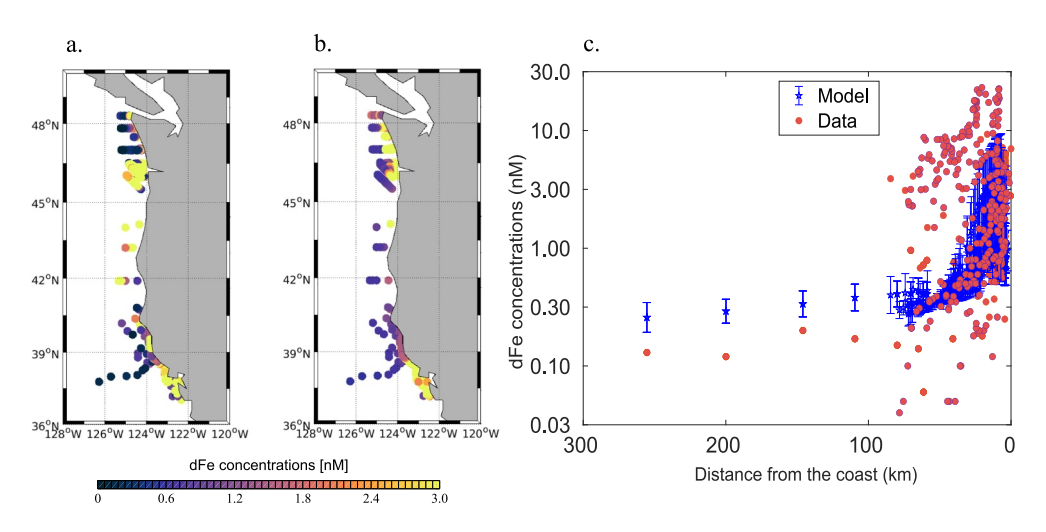


Figure 1. Observed and modeled dissolved iron (dFe, nM) in the upper 100 m depth. (a) Observations from a U.S. West Coast Fe data compilation (see Section 2.3). (b) Annual mean average dFe concentrations from the model, sampled at the same location as for observations. (c) Observed versus modeled dissolved Fe concentrations at the ocean surface as a function of the distance from the coast line. Model output is sampled at the same locations and months as for observations. Error bars around the blue-dot points show the standard deviation of the model results.

the cross-shelf transport driven by transient eddies. Note that all quantities in Equations 5–8 represent temporal and alongshore averages. Furthermore, to facilitate the interpretation of transient terms, we combine the contribution of time-dependent, coast-wide fluctuations $(\overline{[u'][Fe']})$ with transient fluctuations that also vary in the alongshore direction $(\overline{[u'*Fe'*]})$. As such, both $\overline{[T^{SE}]}$ and $\overline{[T^{TE}]}$ arise from correlations between u and Fe, solely in space for the former and in time for the latter. To simplify the notation in the rest of the paper, we drop the averaging operators (i.e., the square brackets and over-bars) and refer to the averaged transport terms in Equations 6–8 as T^{MM} (mean transport), T^{SE} (standing eddies and meanders), and T^{TE} (transient eddies), respectively, unless specified otherwise. We estimate these quantities from model output, following the approach detailed in Appendix A.

3. Results

3.1. Evaluation of the Model, With a Focus on Dissolved Fe

An extensive validation of the model against in situ and remote sensing data, based on the "parent" 4-km U.S. West Coast simulation, is presented in Deutsch et al. (2021) and Renault et al. (2021), showing good agreement for both hydrographic and dynamical properties. A further assessment of the characteristics and dynamics of the California Undercurrent is presented in Chen et al. (2021). The 1-km resolution simulations discussed here are broadly similar to the "parent" simulation; in Supporting Information S1 we provide an additional validation for physical and biogeochemical properties that directly influence the shelf-to-basin Fe transport: dissolved $\rm O_2$ patterns (Figures S2 and S3 in Supporting Information S1) and the California Undercurrent (Figure S4 in Supporting Information S1).

Overall, the model spatial patterns and seasonal variability for dissolved O_2 concentrations fall within the range of the observations (Figures S2 and S3 in Supporting Information S1). The Undercurrent flows faster in the southern part of the domain (in particular, south of the Heceta Bank, Figure S4 in Supporting Information S1) and flows nearly continuously along the coast, as suggested by observations (Pierce et al., 2000). We also note a significant seasonal variability, with shoaling and strengthening of the Undercurrent through the Fall and Winter (Thomson & Krassovski, 2010) (Figure S5 in Supporting Information S1). In the following, we further provide an in-depth evaluation of the model dFe against the new U.S. West Coast dFe compilation.

In general, the model captures the magnitude and spatial variability of observed Fe (Figure 1). Along the coast, both model and observations show high dFe concentrations in the upper ocean, reflecting intense benthic release from the shallow bathymetry. In the open ocean, dFe concentrations are low in both model and observations,

PHAM ET AL. 6 of 19

reflecting limited external Fe inputs, sustained biological uptake, and scavenging. Away from the coast, model dFe concentrations are low at the surface (~0.3 nM) because of biological uptake, and gradually increase in subsurface waters following remineralization (>1 nM).

Compared to observations, the model underestimates the sharp gradient and variability in dFe between coastal and open ocean waters (Figure 1c). Along the shelf, observed dFe values vary between 0.03 and 30 nM, while model dFe values show a somewhat reduced range between 0.2 and 10 nM. In the open ocean, the model tends to overestimate dFe concentrations, while it struggles to capture extremely low dFe in shallow layers, producing a more uniform dFe distribution than observed. This bias is likely caused by our model exclusion of fluvial Fe sources and the model Fe scavenging scheme, which represents Fe protection by organic ligands with a uniform ligand concentration of around 0.6 nM, a common assumption for ocean biogeochemical models (Tagliabue et al., 2016).

While low compared to typical values for macro-nutrients, the correlation coefficient between modeled and observed dFe (R = 0.25) is in the upper range of global ocean biogeochemical models (Tagliabue et al., 2016), which can show correlation coefficients as low as 0.10 or even negative, reflecting limited ability to capture the complexity of Fe cycling. Comparing to global models, our high-resolution regional model produces more realistic cross-shore gradient in dFe, despite somewhat underestimating the range of observations (Figure 1c). Multiple reasons are likely behind this bias—including simplifications in the Fe protection and scavenging schemes. We also note that comparison of climatological model values versus instantaneous measurements is likely to underestimate the range captured by observations, which are taken at different times of the year, and are affected by eddies and other sources of variability.

3.2. Fate of Sediment-Derived Fe

Analysis of the model Fe budget shows that benthic release is the dominant source of Fe along the northern U.S. West Coast (Figure S1 in Supporting Information S1). On the shelf, 97% of external Fe inputs is from the sediment. Benthic release is then the dominant source of dFe (4.80 vs. 0.01 mol s⁻¹ from atmospheric deposition), the majority of which (3.79 mol s⁻¹) is retained on the shelf by a combination of biological uptake, scavenging, and transport to the sediment by sinking particles. Scavenging onto particles removes the majority of Fe inputs (3.55/4.81 = 74%), consistently with global model results. (J. K. Moore & Braucher, 2008) (Figure 2).

Our results update the picture presented in Siedlecki et al. (2012), which suggested a dominant role for biological uptake in consuming benthic-derived dFe (\sim 80%), and limited scavenging (\sim 0.05%) on the shelf. These differences reflect the increased realism and complexity of Fe biogeochemistry—in particular scavenging—in our model (J. K. Moore et al., 2004).

Analysis of the dFe balance over the shelf and open ocean (up to a distance of 400 km from the coast) (Figure 2) shows that the shelf-to-basin transport is one of the two major inputs of dFe to the open ocean (0.94 mol s⁻¹), second only to vertical supply (1.63 mol s⁻¹), despite the narrow surface area of the shelf compared to the open-ocean. The cross-shelf flux represents 36% (0.94/2.62) of the total dFe input to the surface open ocean, far exceeding dust deposition (0.05 mol s⁻¹). It is also larger than the net biological uptake offshore (0.11 mol s⁻¹), suggesting that the continental shelf is a source of Fe to the broader Northeast Pacific.

3.3. The Shelf-To-Basin Transport of Fe

3.3.1. Structure and Drivers of the Shelf-To-Basin Fe Transport

Two pathways dominate Fe transport from the shelf to the open ocean: the first in the SBL and the second in the BBL (Figure 3a). These pathways are the result of the wind-driven overturning circulation that develops on the continental shelf (Figure 3b) (Damien et al., 2023). The patterns and seasonal variability of this cross-shelf overturning show a complex three-dimensional structure (Figure S5 in Supporting Information S1) that is influenced both by variations in surface winds and by interactions between the poleward California Undercurrent (Figure S4 in Supporting Information S1) and bottom topography.

In the SBL, the seasonal cross-shelf overturning consists of offshore transport during upwelling and inshore transport during downwelling and relaxation events, balanced by currents with opposite directions in the water column interior (Figure S5 in Supporting Information S1). In contrast, the mean circulation is directed

PHAM ET AL. 7 of 19

19449224, 2024, 5, Downloaded

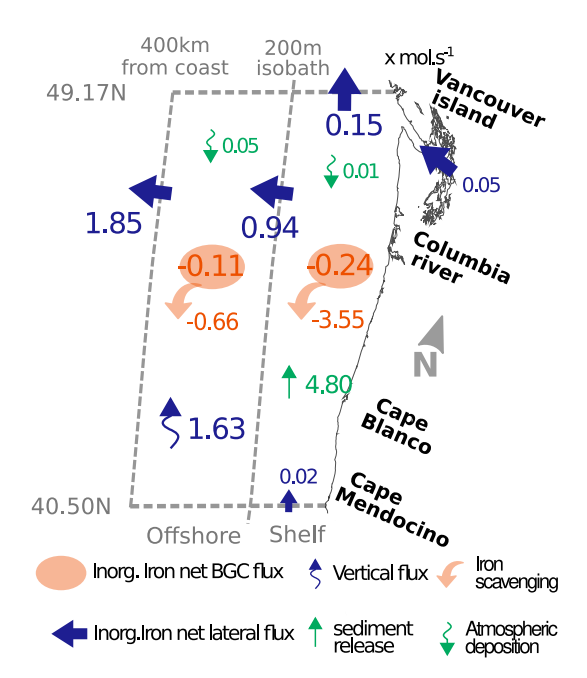


Figure 2. Schematic of the balance between physical transport and biogeochemical processes for dissolved Fe (dFe) along the northern U.S. West Coast. The balance reflects an average over the 9-year period from 2008 to 2016. Biogeochemical sources and sinks and transport rates of dissolved Fe are integrated over the shelf region (defined by the 200 m isobath) and the open-ocean region (up to a distance of 400 km from the coast, between the surface and 200 m depth). Green arrows show external sources of dFe (atmospheric deposition and benthic release); blue arrows show horizontal and vertical physical transport; and red circles show net biogeochemical transformation rates, that is, the sum of uptake by phytoplankton, and release by remineralization. Removal by scavenging, which ultimately transports Fe to the sediment as sinking particles, is indicated by a red arrow. Units are mol s⁻¹. The integrated cross-shore transport of dFe is 0.94 mol s⁻¹.

offshore year-round in the BBL. This can be attributed to the frictional dynamics of the California Undercurrent, which, despite a shoaling and intensification in the fall (Chen et al., 2021), continuously moves waters poleward through the year (Figures S4 and S5 in Supporting Information S1). Transport in the BBL emerges as a downhill flow with both offshore and downward components, which peaks in magnitude over the outer shelf. Notably, the magnitude of the California Undercurrent and of the downhill flow in the BBL are strongly correlated, especially at the location of the 200 m isobath, reflecting their dynamical connection.

Despite the good correlation between the cross-shore Fe flux (Figure 3a) and the cross-shelf currents (Figure 3b), notable differences between the water volume and Fe transport are observed, mainly in the water column interior outside the boundary layers. While the SBL Fe transport pathway is active mostly during the upwelling season from spring to summer, reversing sign in winter, the BBL pathway is active throughout the year, although it is intensified in the wake of upwelling events (August–October, Figure 3a). Relative to the two boundary layers, the mean Fe transport in the water column interior remains small, and mostly directed offshore, in contrast with the mean volume transport (Figure 3b).

Our results also suggest that intense dFe export follows upwelling events, but the BBL pathway is active year-round on the continental shelf and upper slope, driven by the persistent downhill tilt of the bottom current (Chen et al., 2021; Damien et al., 2023). As discussed further in Section 3.3.3, this finding is also consistent with the results of Siedlecki et al. (2012), which suggest that in addition to when the wind relaxes and reverses after upwelling events, the Fe-laden BBL is mixed into the water column and transported offshore along isopycnals most efficiently where the poleward undercurrent intersects the upper slope near the shelf break, and with the intensity of the undercurrent. Integrated along the shelf break, using an average thickness for both boundary layers of 25 m, we find that 19% of the cross-shore Fe flux takes place in the SBL (0.18 mol s⁻¹) and 46% (0.43 mol s⁻¹) in the BBI

Vigorous cross-shore Fe transport takes place during the entire upwelling season. However, the peak Fe transport is observed in September (Figure 3c), a 2-month lag from the peak in the cross-shore volume transport (Figure 3d) and 1-month lag from the peak in the benthic dFe release associated with a minimum in bottom O_2 concentrations on the shelf (Figures 3e and 3f). More generally, the seasonal cycle of the shelf-to-basin Fe transport arises from the interaction between the volume transport flux (Figure 3b), benthic dFe release (Figure 3e), and bottom O_2 concentrations (Figure 3f). In particular, bottom O_2 concentrations on the continental shelf dictate the magnitude of the benthic dFe release, which in combination with the magnitude and timing of the volume transport flux, shape the seasonal cycle of the shelf-to-basin Fe transport.

3.3.2. Contribution of Transient and Standing Eddies to the Variability of the Shelf-To-Basin Fe Transport

Additional differences between the mean Fe and volume transports, in particular in the water column interior, can be attributed to the role of transient and standing eddies. A decomposition of the cross-shore Fe transport (Figure 3a) into different components reflecting respectively the large-scale mean circulation (T^{MM}), standing eddies and meanders (T^{SE}), and transient eddies (T^{TE}) reveals a substantial influence of fine-scale circulation on the exchange of Fe from the shelf to the open ocean (Figure 4a). As a whole, standing and transient eddies intensify the mean offshore Fe transport at the surface, and oppose it near the bottom. Notably, eddies also oppose the mean Fe transport in the water column interior, where their combined effect—always directed offshore—overcomes the net inshore transport by the mean circulation, resulting in a net Fe export from the shelf to the open ocean.

PHAM ET AL. 8 of 19

19449224, 2024, 5, Downloaded from https://agupubs.onlinelibrary.wiley.com/doi/10.10292023GB008029 by University Of California, Los, Wiley Online Library on [08/05/2024]. See the Terms and Conditions (https://online.com/doi/10.1029/2023GB008029).

ditions) on Wiley Online Library for rules of use; OA articles are governed by the applicable Cres

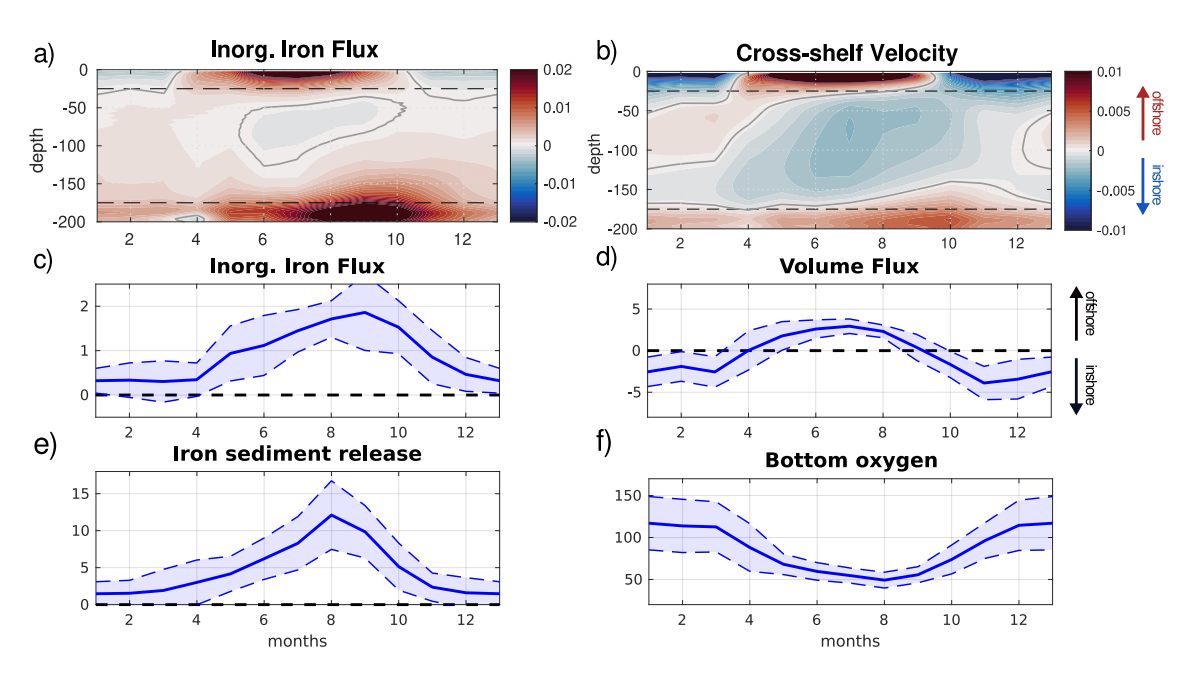


Figure 3. Seasonal cycle of the processes governing the transport of dissolved Fe from the shelf to the open ocean. (a) Climatological cross-shore Fe transport $(10^{-6} \text{ mol m}^{-2} \text{s}^{-1})$ as a function of depth and time, averaged along the 200 m isobath. This transport flux is calculated as [T] = [uFe], following the approach discussed in Section 2.4.2. Positive values (red colors) show transport directed offshore; negative values (blue colors) show transport directed inshore. (b) Same as (a) but for the cross-shore current velocity (m s⁻¹). (c) Climatological cross-shore Fe transport (mol s⁻¹) integrated by depth and distance along the 200 m isobath. (d) Climatological cross-shore volume transport ($10^{5} \text{ m}^{3} \text{s}^{-1}$). (e) Climatological benthic Fe flux (mol s⁻¹) integrated over the continental shelf. (f) Bottom O₂ concentration (mmol m⁻³) averaged over the continental shelf. Positive values in (c) and (d) show transport directed offshore.

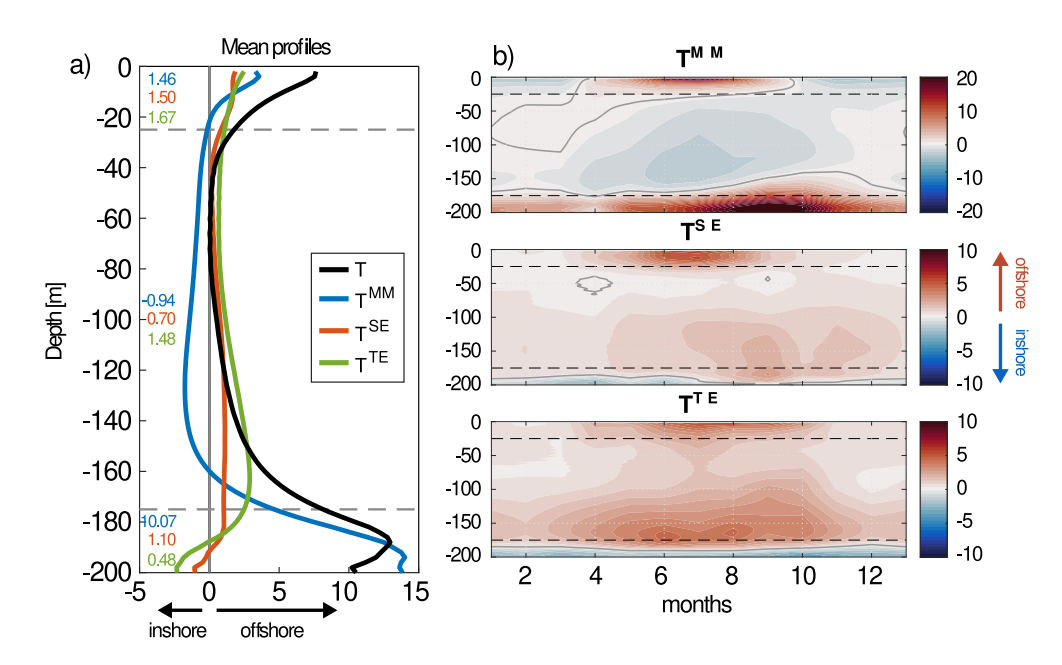


Figure 4. Role of mean circulation and eddies for the shelf-to-basin Fe transport. (a) The total cross-shelf Fe flux (T, black) is decomposed into mean (T^{MM}, blue) , standing eddy $(T^{\text{SE}}, \text{red})$, and transient eddy (T^{TE}, green) components. All fluxes have been averaged over time and along the 200 m isobath. Section 2.4.2, Equations 5–8 provide definitions for the different flux terms, with further details in Appendix A. Positive values indicate transport directed offshore, and negative values transport directed inshore. Units for all fluxes are 10^{-9} mol m⁻²s⁻¹. The average value of the different components within the surface boundary layer (SBL, top), interior (center), and bottom boundary layer (BBL, bottom) are annotated on the figure. (b) Seasonal cycle of the different components of the cross-shore Fe flux averaged along the 200 m isobath $(10^{-9} \text{ mol m}^{-2}\text{s}^{-1})$: T^{MM} (upper panel), T^{SE} (middle panel), and T^{TE} (lower panel).

PHAM ET AL. 9 of 19

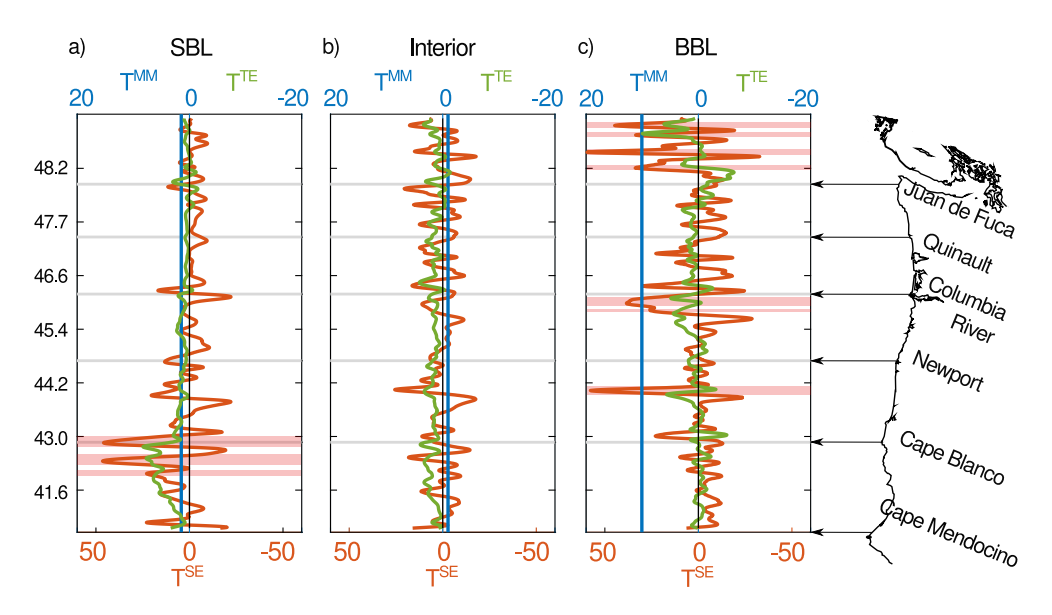


Figure 5. Alongshore variability and hot-spots in the shelf-to-basin Fe transport. Vertically and time-averaged cross-shelf Fe transport (a) over the surface boundary layer (SBL, 0–25 m depth), (b) the water column interior (25–175 m depth), and (c) the bottom boundary layer (BBL, 175–200 m depth). The total cross-shelf Fe flux is decomposed into its monthly mean (T^{MM} , blue), standing eddy (T^{SE} , red), and transient eddy (T^{TE} , green) components. Note that, in this figure, to visualize the alongshore variability of the eddy components, the alongshore averaging filter is not applied. More precisely, \overline{T}^{MM} , \overline{T}^{SE} , and \overline{T}^{TE} are shown. Units for all fluxes are 10^{-9} mol m⁻² s⁻¹. Positive values indicate offshore transport; negative values inshore transport. The shaded red boxes highlight hot-spots of cross-shore Fe transport (here defined as total Fe flux larger than $30 \cdot 10^{-9}$ mol m⁻² s⁻¹). In all panels, the thin vertical black line shows zero fluxes.

In the SBL (0–25 m), the eddy terms T^{TE} and T^{SE} are positive, and, when combined, larger than T^{MM} . Each contributes to about one-third of the total SBL Fe transport (Figure 4a). In contrast, T^{MM} dominates the Fe transport in the BBL (approximately 175–200 m depth), where T^{SE} and T^{TE} are nearly one order of magnitude smaller. However, the direction of eddy transport terms changes between the upper part of the BBL, where they are directed offshore, and the lower part, where they are directed inshore, and thus oppose T^{MM} . In the upper BBL, both T^{SE} and T^{TE} represent a substantial contribution to the total Fe flux from the shelf to the open ocean (\sim 50%). In contrast, in the lower BBL, they reduce the offshore Fe transport by \sim 30%. Away from the boundary layers, T^{SE} and T^{TE} oppose the T^{MM} , resulting in a weakly positive offshore transport of Fe in the water column interior.

The mean and eddy components of the cross-shore Fe transport show significant temporal variability following the seasonal cycle of upwelling. This seasonal variability is more pronounced in the boundary layers, in particular for the mean component T^{MM} (Figure 4b), which shows reversals in direction similar to the volume transport (Figure 3b). In contrast, eddy components are generally weakly enhanced during upwelling (Figures 4c and 4d). The nearly year-round activity of the T^{MM} and T^{SE} in the BBL can be attributed to the downslope tilt of the California Undercurrent (Chen et al., 2021; Damien et al., 2023). In addition, the intensification of the offshore BBL flow from August to October coincides with the seasonal intensification of the California Undercurrent (Chen et al., 2021; Thomson & Krassovski, 2010).

A coast-wide analysis of the cross-shore Fe flux (Figure 5) reveals the presence of significant local hot-spots of cross-shelf Fe exchange, in particular near the surface and the bottom. These hot-spots, shown by local maxima in $T^{\rm SE}$, are mainly driven by locally intensified transport by standing eddies (red lines in Figure 5), reflecting the presence of meanders or separations of the alongshore current that enhance exchange across the shelf break. To a lesser extent, we also observe hot-spots driven by locally intensified transient eddies, although their magnitude and spatial variability are smaller than for standing eddies.

In the SBL, we highlight the region south of Cape Blanco as the main pathway of surface Fe export, with two large peaks near Cape Sebastian (42.35°N) and Cape Blanco (42.83°N). This standing-eddy export pathway, further intensified by transient eddies, is likely fueled by strong, localized upwelling along the Northern California coast (Damien et al., 2023). A secondary region of enhanced Fe export is located near the Columbia River estuary.

PHAM ET AL. 10 of 19

In the BBL, multiple hot-spots of Fe transport are linked to the coastal bathymetry, which in turns dictates the location of meanders in the mean bottom current. Three major hot-spots are located at the southern edge of the Heceta Bank (43.95°N), the Nehalem Bank (45.95°N–46.40°), and the Northern Juan de Fuca Canyon (48.23–48.50N). The cross-shore Fe flux by standing eddies there exceeds $30 \cdot 10^{-9}$ mol m⁻² s⁻¹. Two secondary hot-spots with smaller offshore transport ($\sim 20 \times 10^{-9}$ mol m⁻² s⁻¹) are located north of Cape Blanco (43°N) and Grays Canyon (47.04°N).

We note that hot-spots of eddy transport could be related to regions of formation of subsurface coherent eddies, which are commonly observed in this region (McCoy et al., 2020; Pelland et al., 2013). The model indeed shows a rich population of subsurface eddies just offshore of the continental slope, particularly during the fall season (Figure S5 in Supporting Information S1). Consistent with their formation by topographic interactions (Molemaker et al., 2015), these subsurface eddies trap Fe-rich BBL waters in their cores (Figure S6 in Supporting Information S1), subsequently transporting Fe offshore, thus contributing to Fe export from the continental shelf.

3.3.3. Contribution of the California Undercurrent to the Shelf-To-Basin Fe Transport

The importance of standing eddies and meanders in driving hot-spots of Fe exchange across the shelf break suggests a major role for the circulation dynamics of the California Undercurrent. Following upwelling, when both the offshore Fe transport and the undercurrent are seasonally the strongest (Figure 3a), we observe a high correlation (R = 0.93) between the alongshore Fe and volume transports along the shelf (Figure 6a). This indicates that alongshore variability of the cross-shore Fe transport, on spatial scale of the order of $10-100 \, \text{km}$, is primarily driven by mean current patterns.

However, alongshore variability in dFe concentrations on the shelf is also important. The progressive increase of the cross-shore Fe flux relative to the volume flux north of Cape Blanco (Figure 6a) reflects a concomitant increase in dFe concentrations on the shelf. These in turn can be explained by larger benthic inputs (Figure 6b) to low- O_2 bottom waters. North of Cape Blanco, the ratio between the Fe and volume flux is much larger for the offshore transport than the inshore transport, confirming the Fe enrichment of shelf waters transported to the open ocean. Thus, recurring low- O_2 conditions on the shelf support high benthic fluxes that increase dFe concentration on the shelf and enhance offshore dFe transport. The influence of high benthic dFe release can be observed on relatively large spatial scales, on the order of 100 km, in particular between 43.5°N and 47.5°N. In contrast, downhill flow in the BBL shapes the shelf-to-basin dFe transport on spatial scales of tens of km.

These considerations apply to the three major hot-spots of Fe export located near the southern Heceta and Nehalem Banks, and the Northern Juan de Fuca Canyon. Here, vigorous dFe export is mainly driven by enhanced volume transport associated with standing eddies and meanders, but with a significant contribution from locally intense release of Fe from low-O₂ sediment. In contrast, at two secondary hot-spots north of Cape Blanco and north of Grays Canyon, benthic Fe inputs are not particularly enhanced relative to the surrounding waters.

On the outer shelf, enhanced volume fluxes correspond to local intensification of the California Undercurrent (Figure 6c). Episodes of detachment of the California Undercurrent from the continental shelf facilitate bottom Fe export in the southern part of the Heceta Bank and the Northern Juan de Fuca Canyon. Topographic features with enhanced curvature, such as headlands, submarine canyons, and banks, promote offshore Fe transport by facilitating separation of the poleward Undercurrent, often followed by instabilities and generation of subsurface eddies that migrate offshore (Molemaker et al., 2015). In contrast, the hot-spot of Fe transport at the Nehalem Bank does not correspond to a significant detachment of the California Undercurrent from the upper slope, suggesting a possible important role for BBL dynamics.

A more direct assessment of the importance of Undercurrent-topographic interactions is provided by analysis of the along-isobath component of the mean flow near the bottom, which we diagnose as $\hat{z} \cdot (\overrightarrow{U}_b \times \overrightarrow{\nabla} H) / |\overrightarrow{\nabla} H|$,

where \hat{z} is the vertical unit vector, $\overrightarrow{U_b}$ the velocity at the bottom, and H the bottom topography. This quantity is positive nearly everywhere, that is, the bottom current flows with the slope to its right (Figure 6d). Larger bottom velocities occur around or just shallower of the 200 m isobath, where the core of the Undercurrent is found closer to the seafloor. These local maxima are closely correlated with intensification of the Undercurrent (Figure 6c). Frictional interactions and mixing generate an Ekman transport in the BBL. We diagnose the cross-isobath component of this Ekman transport as $-\frac{1}{pf}\hat{z}\cdot\overrightarrow{\tau_b}\times\overrightarrow{\nabla}H/|\overrightarrow{\nabla}H|$ (Figure 6e), where ρ is the density, f the Coriolis

PHAM ET AL.

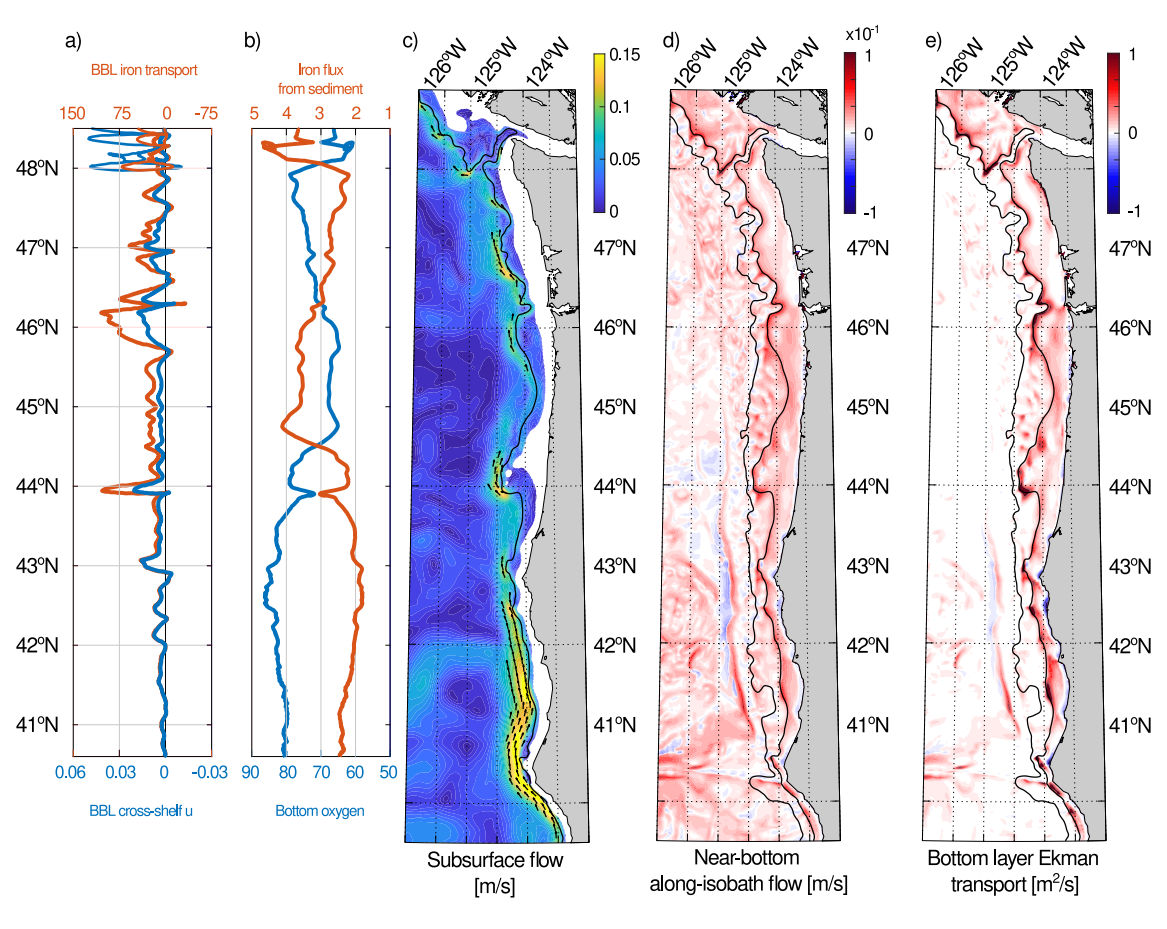


Figure 6. Role of the California Undercurrent for cross-shelf Fe transport in the bottom boundary layer (BBL). (a) Time-averaged Fe transport $(10^{-9} \text{ mol m}^{-2} \text{s}^{-1}, \text{ solid red line})$ and cross-shelf velocity (m s⁻¹, solid blue line) in the BBL between August and October. This period coincides with an intensification of both the poleward California Undercurrent and the related BBL transport that support enhanced Fe fluxes (see also Figure 3). (b) Time averaged Fe release from the sediment $(10^{-10} \text{ mol m}^{-2} \text{s}^{-1}, \text{ solid red line})$ and bottom O_2 concentrations (mmol m⁻³, solid blue line) along the 200 m isobath between August and October. (c) Mean horizontal currents averaged in the 100–300 m layer between August and October. Colors show the current velocity; arrows the current direction, for speed above 0.08 m s^{-1} . The black solid line shows the 200 m isobath. (d) Along-isobath component of the mean flow (m s⁻¹) near the bottom. Positive values (red colors) indicate a flow with the slope to its right. (e) Ekman transport (m² s⁻¹) in the BBL. Positive values (red colors) indicate downhill Ekman transport. In (d) and (e), the black solid lines show the 200 and 1,000 m isobaths.

term, and $\vec{\tau}_b$ the mean current stress at the bottom. Along the shelf, the mean Ekman transport in the BBL is directed downhill, and peaks around or just above the 200 m isobath, reflecting a more intense drag from the poleward Undercurrent. Averaged between isobaths 150 and 250 m, the alongshore bottom poleward current and downhill Ekman transport are significantly correlated (R = 0.91). Furthermore, local maxima in the downhill Ekman transport are generally co-located with Fe transport hot-spots (Figure 6a). In addition, considering a BBL thickness of 25 m, the average mean velocity within the BBL at the hot-spot locations ranges from 0.02 to 0.04 m s⁻¹. These relatively large velocities suggest that the downslope Ekman transport caused by the Undercurrent plays a major role in transport of Fe away from the continental shelf.

4. Discussion and Conclusions

Our high-resolution simulations reveal that the continental shelf of the U.S. West Coast is a major source of Fe for the North Pacific Ocean. The majority of this Fe is locally released by the sediment under low- O_2 conditions. While most of this Fe (3.55/4.81 = 74%) is scavenged by sinking particles, or biologically taken up on the shelf, a substantial fraction (0.94/4.81 \sim 20%) escapes removal and is transported offshore by a combination of mean and eddy currents, ultimately enhancing primary production in the strongly Fe-limited open-ocean environment.

We highlight two main pathways for the shelf-to-basin Fe transport along the northern U.S. West Coast. The first, in the SBL, is responsible for 19% of the total transport, and is mostly active during upwelling. The second, in the

PHAM ET AL. 12 of 19

BBL, is responsible for 46% of the total transport and is active year-round. These findings are consistent with results by Siedlecki et al. (2012), further emphasizing the dynamics of the California Undercurrent and its interactions with the seafloor. Amplification of BBL Fe transport in the wake of upwelling reflects a combination of more vigorous bottom currents, and more intense benthic Fe release under seasonal hypoxia (Severmann et al., 2010).

Several hot-spots of cross-shelf Fe exchange can be observed along the coast, driven by meanders of the California Undercurrent, and enhanced by local maxima in benthic Fe release in low-O₂ bottom waters. Standing and transient eddies contribute each to about one-third of the total Fe transport in the SBL, and increase transport in the BBL by nearly 50%. In the water column interior, eddies oppose the mean circulation, sustaining net offshore Fe transport despite the mean upwelling circulation directed inshore.

While model biases remain, a realistic representation of the cross-shore dissolved Fe gradients and fine-scale circulation along the shelf (Damien et al., 2023) suggests that our findings are robust to model assumptions and can be qualitatively extended to other productive margins with similar circulation and low-O₂ conditions. Release from the sediment is a dominant source of Fe not only in the California Current, but also in other EBUS and low-O₂ continental margins (Elrod et al., 2004; Johnson et al., 1999; Lam et al., 2006; T. Liu et al., 2022; Severmann et al., 2010). Because of the widespread distribution of coastal low-O₂ environments (Breitburg et al., 2018; Fennel & Testa, 2019) benthic Fe fluxes from continental margins likely impacts primary production in both nearshore and offshore waters over vast parts of the global ocean (Elrod et al., 2004; Johnson et al., 1999; Lam et al., 2006; T. Liu et al., 2022; Severmann et al., 2010). Extrapolating our findings for the U.S. West Coast, we argue that a better characterization of the fine-scale mechanisms controlling the shelf-to-basin Fe transport is crucial for understanding variability in oceanic primary production and to improve ocean biogeochemical models from regional to global scales (Boyd & Tagliabue, 2015; Tagliabue, Williams, et al., 2014; Tagliabue et al., 2016).

Recent studies based on observations (Wong et al., 2022) and models (Misumi et al., 2021) suggest the presence of preferential export pathways for shelf-derived Fe in the North Pacific, facilitated by protection by organic ligands and interaction with slowly sinking particles. A more sophisticated representation of Fe sources and ligand dynamics in our model would likely improve its ability to capture the observed range of Fe variability. This would lead to higher Fe concentrations and stronger gradients, and potentially greater transport than currently found, in particular by eddies. Thus, the quantitative results presented here should be interpreted cautiously and are likely to represent a lower bound for the magnitude of the shelf-to-basin Fe transport of the real ocean.

More importantly, our results expand previous findings on the importance of fine-scale circulation from other basins, such as subarctic Pacific, subtropical Atlantic, and the Southern Ocean, which highlighted the role of eddies in the delivery of dFe and macronutrients from continental margins to the open ocean (Conway et al., 2018; Fiechter & Moore, 2012; Frenger et al., 2018; Jersild et al., 2021; Lovecchio et al., 2022; St-Laurent et al., 2019). We emphasize the importance of mesoscale and submesoscale currents to enhance or counterbalance the mean circulation, not just in the open ocean, but specifically on the continental shelf where Fe inputs are greatest. These fine-scale circulation patterns not only include transient eddies and cross-shelf meanders in the prevailing currents but also subsurface coherent eddies (Pelland et al., 2013) that trap Fe-laden BBL waters (Molemaker et al., 2015) and transport them offshore, often hundreds to thousands km away from the margins where they originate from McCoy et al. (2020). A clear separation of the transport by subsurface coherent eddies from that of other transient eddies would require detecting and tracking them in model output (Frenger et al., 2018). We also note that our model configuration does not include tidal motions, which would cause a tidal rectification of advective Fe transport—that is, a net Fe flux averaged over a tidal cycle—and increased vertical mixing near the bottom, potentially enhancing the shelf-to-basin transport. We leave a detailed analysis of these dynamics to future work.

The physical and biogeochemical processes that govern the shelf-to-basin Fe transport, such as benthic release and biological uptake, are likely to undergo significant changes in a future climate, following widespread oceanic warming, changes in circulation, and O_2 loss (Kwiatkowski et al., 2020; T. Liu et al., 2022; Wallmann et al., 2022). In addition, the shelf-to-basin pathways described here are expected to affect the cross-shore transport of non-dissolved Fe pools (in particular suspended Fe minerals), as well as other trace elements (Richon et al., 2020; Weber et al., 2018), which can also modulate primary production in far-field regions. We argue that future studies should combine an improved representation of Fe cycle processes—in particular ligand and particulate dynamics—with a more accurate understanding of the small-scale physical circulation along continental margins, as informed by high-resolution models and observational campaigns. In turn, a correct

PHAM ET AL. 13 of 19

representation of the shelf-to-basin transport of Fe, trace metals, and other limiting nutrients is essential to improve current models used for ocean biogeochemistry and climate change studies (Tagliabue et al., 2016, 2020).

Appendix A: Eddy Decomposition of the Fe Transport and Online Computation

Following the approach by Lee and Coward (2003), we diagnose the spatial and temporal variabilities of the shelf-to-basin Fe transport flux by deposing it into a mean flux plus two eddy-induced fluxes. The approach involves two low-pass filters, one in time and one in space, as described in the main text. First, the cross-shelf Fe flux, T = u Fe is decomposed into time mean and fluctuating components as:

$$u = \overline{u} + u'$$
 and $Fe = \overline{Fe} + Fe'$, (A1)

We then apply a spatial decomposition into alongshore mean and alongshore variations to the temporal mean component Equation A2 or to both components Equation A3 as:

$$u = \overline{[u]} + \overline{u^*} + u'$$
 and $Fe = \overline{[Fe]} + \overline{Fe^*} + Fe'$ (A2)

or

$$u = \overline{[u]} + \overline{u^*} + [u'] + u'^*$$
 and $Fe = \overline{[Fe]} + \overline{Fe^*} + [Fe'] + Fe'^*$ (A3)

Here, by construction, $\overline{u'} = 0$, $\overline{Fe'} = 0$, $[u^*] = 0$, and $[Fe^*] = 0$, so that the transport T = u Fe has the following property:

$$\overline{uFe} = \overline{u}\overline{Fe} + \overline{u'Fe'} \tag{A4}$$

$$[uFe] = [u][Fe] + [u^*Fe^*]$$
 (A5)

Therefore, the alongshore and temporal mean Fe transport, $[\overline{T}]$, is simply:

$$[\overline{T}] = [\overline{u}\overline{Fe}] = [\overline{u}][\overline{Fe}] + [\overline{u}^*\overline{Fe}^*] + [\overline{u'Fe'}]$$
 from A2 (A6)

or

$$[\overline{T}] = [\overline{u}Fe] = [\overline{u}][\overline{Fe}] + [\overline{u}^*\overline{Fe}^*] + [\overline{u'}|\overline{Fe'}] + [\overline{u'*Fe'*}]$$
 from A3 (A7)

We further define the mean, standing eddy, and transient eddy transport terms as:

$$\left[\overline{T^{MM}}\right] = \left[\overline{u}\right]\left[\overline{Fe}\right] \tag{A8}$$

$$\left[\overline{T^{\text{SE}}}\right] = \left[\overline{u}^* \overline{Fe}^*\right] \tag{A9}$$

$$\left[\overline{T^{TE}}\right] = \left[\overline{u'Fe'}\right] = \overline{\left[u'\right]\left[Fe'\right]} + \left[\overline{u'^*Fe'^*}\right] \tag{A10}$$

As discussed in the main text, $\left[\overline{T^{MM}}\right]$ is the cross-shelf Fe transport caused by the climatological mean circulation and Fe distribution, $\left[\overline{T^{SE}}\right]$ is the cross-shelf transport caused by meanders and standing eddies that intersect the shelf break, and $\left[\overline{T^{TE}}\right]$ is the cross-shelf transport caused by transient eddies.

A caveat of this approach is the need to save *u* and *Fe* at a frequency high enough to capture the variability allowed by the temporal and spatial resolution of the model (i.e., submesoscale). Considering the long duration of the

Acknowledgments

Funding for this work was provided by the

US National Science Foundation, Grants

OCE-2023493 and OCE-1847687 to DB.

This work used the Expanse system at the

San Diego Supercomputer Center through

allocation TG-OCE170017 from the Advanced Cyber infrastructure

Coordination Ecosystem: Services and

Support (ACCESS) program, which is supported by National Science Foundation

Grants 2138259, 2138286, 2138307,

2137603, and 2138296.

simulations needed to achieve statistically robust results, on the order of several years or longer, this implies high output storage requirements that are currently unfeasible. To overcome this limitation, we compute and average T, u, and Fe online, as the model runs, and save them at daily frequency. This allows us to capture signals at frequencies as high as captured by the model. Then, we compute the terms in the eddy decomposition offline by difference, applying the flux formulation on filtered u and Fe as:

$$\begin{split} T &= T^{MM} + T^{\text{SE}} + T^{TE} \\ T^{MM} &= \left[\overline{u} \right] \left[\overline{Fe} \right] \\ T^{\text{SE}} &= \overline{u} \, \overline{Fe} - \left[\overline{u} \right] \left[\overline{Fe} \right] \\ T^{TE} &= T - \overline{u} \, \overline{Fe} \end{split}$$

Data Availability Statement

The ROMS-BEC model code used to generate the simulations can be found on the Zenodo repository, under the following DOI: Kessouri et al. (2022) (Version v2) [model code]: https://doi.org/10.5281/zenodo.6886319. Model results reported in the paper are reproducible using the setup and forcing described. Since the model outputs are too big (even with only iron-related variables, model outputs are >500 GB in size), we were unfortunately not be able to directly deposit them into a public repository. Please contact the corresponding author (anhlpham78@ucla.edu) if you have any question or request. The compilation of Fe observations along the US West Coast can be found on the Zenodo repository, under the following DOI: https://doi.org/10.5281/zenodo. 11068852.

References

Armstrong, R. A., Lee, C., Hedges, J. I., Honjo, S., & Wakeham, S. G. (2001). A new, mechanistic model for organic carbon fluxes in the ocean based on the quantitative association of POC with ballast minerals. *Deep Sea Research Part II: Topical Studies in Oceanography*, 49(1), 219–236. https://doi.org/10.1016/S0967-0645(01)00101-1

Biller, D. V., & Bruland, K. W. (2013). Sources and distributions of Mn, Fe, Co, Ni, Cu, Zn, and cd relative to macronutrients along the central California coast during the spring and summer upwelling season. *Marine Chemistry*, 155, 50–70. https://doi.org/10.1016/j.marchem.2013.06.003

Biller, D. V., Coale, T. H., Till, R. C., Smith, G. J., & Bruland, K. W. (2013). Coastal iron and nitrate distributions during the spring and summer upwelling season in the central California current upwelling regime. *Continental Shelf Research*, 66, 58–72. https://doi.org/10.1016/j.csr.2013.

Boiteau, R. M., Till, C. P., Coale, T. H., Fitzsimmons, J. N., Bruland, K. W., & Repeta, D. J. (2019). Patterns of iron and siderophore distributions across the California current system. *Limnology & Oceanography*, 64(1), 376–389. https://doi.org/10.1002/lno.11046

Boyd, P. W., & Ellwood, M. J. (2010). The biogeochemical cycle of iron in the ocean. *Nature Geoscience*, 3(10), 675–682. https://doi.org/10.1038/ngeo964

Boyd, P. W., & Tagliabue, A. (2015). Using the L* concept to explore controls on the relationship between paired ligand and dissolved iron concentrations in the ocean. *Marine Chemistry*, 173, 52–66. https://doi.org/10.1016/j.marchem.2014.12.003

Breitburg, D., Levin, L. A., Oschlies, A., Grégoire, M., Chavez, F. P., Conley, D. J., et al. (2018). Declining oxygen in the global ocean and coastal waters. *Science*, 359(6371), eaam7240. https://doi.org/10.1126/science.aam7240

Buck, K. N., Selph, K. E., & Barbeau, K. A. (2010). Iron-binding ligand production and copper speciation in an incubation experiment of Antarctic Peninsula shelf waters from the Bransfield Strait, Southern Ocean. *Marine Chemistry*, 122(1–4), 148–159. https://doi.org/10.1016/j.marchem.

Bundy, R. M., Abdulla, H. A., Hatcher, P. G., Biller, D. V., Buck, K. N., & Barbeau, K. A. (2015). Iron-binding ligands and humic substances in the San Francisco Bay estuary and estuarine-influenced shelf regions of coastal California. *Marine Chemistry*, 173, 183–194. https://doi.org/10.1016/j.marchem.2014.11.005

Bundy, R. M., Biller, D. V., Buck, K. N., Bruland, K. W., & Barbeau, K. A. (2014). Distinct pools of dissolved iron-binding ligands in the surface and benthic boundary layer of the California current. *Limnology & Oceanography*, 59(3), 769–787. https://doi.org/10.4319/lo.2014.59.3.0769
Bundy, R. M., Jiang, M., Carter, M., & Barbeau, K. A. (2016). Iron-binding ligands in the southern California current system: Mechanistic studies. *Frontiers in Marine Science*, 3. https://doi.org/10.3389/fmars.2016.00027

Capet, X., McWilliams, J. C., Molemaker, M. J., & Shchepetkin, A. F. (2008). Mesoscale to submesoscale transition in the California current system. Part I: Flow structure, eddy flux, and observational tests. *Journal of Physical Oceanography*, 38(1), 29–43. https://doi.org/10.1175/ 2007JPO3671.1

Chappell, P. D., Armbrust, E. V., Barbeau, K. A., Bundy, R. M., Moffett, J. W., Vedamati, J., & Jenkins, B. D. (2019). Patterns of diatom diversity correlate with dissolved trace metal concentrations and longitudinal position in the northeast pacific coastal-offshore transition zone. *Marine Ecology Progress Series*, 609, 69–86. https://doi.org/10.3354/meps12810

Chase, Z., Johnson, K. S., Elrod, V. A., Plant, J. N., Fitzwater, S. E., Pickell, L., & Sakamoto, C. M. (2005). Manganese and iron distributions off central California influenced by upwelling and shelf width. *Marine Chemistry*, 95(3), 235–254. https://doi.org/10.1016/j.marchem.2004.09.006

Chase, Z., Strutton, P. G., & Hales, B. (2007). Iron links river runoff and shelf width to phytoplankton biomass along the U.S. West Coast. Geophysical Research Letters, 34(4), L04607. https://doi.org/10.1029/2006GL028069

Chase, Z., van Geen, A., Kosro, P. M., Marra, J., & Wheeler, P. A. (2002). Iron, nutrient, and phytoplankton distributions in Oregon coastal waters. Journal of Geophysical Research, 107(C10), 38-1–38-17. https://doi.org/10.1029/2001JC000987

PHAM ET AL. 15 of 19

- Chen, R., McWilliams, J. C., & Renault, L. (2021). Momentum governors of California undercurrent transport. *Journal of Physical Oceanography*, 51(9), 2915–2932. https://doi.org/10.1175/JPO-D-20-0234.1
- Conway, T. M., & John, S. G. (2014). Quantification of dissolved iron sources to the North Atlantic Ocean. Nature, 511(7508), 212–215. https://doi.org/10.1038/nature13482
- Conway, T. M., Palter, J. B., & de Souza, G. F. (2018). Gulf stream rings as a source of iron to the North Atlantic subtropical gyre. *Nature Geoscience*, 11(8), 594–598. https://doi.org/10.1038/s41561-018-0162-0
- Cravatte, S., Kestenare, E., Marin, F., Dutrieux, P., & Firing, E. (2017). Subthermocline and intermediate zonal currents in the tropical pacific ocean: Paths and vertical structure. *Journal of Physical Oceanography*, 47(9), 2305–2324. https://doi.org/10.1175/jpo-d-17-0043.1
- Dale, A. W., Nickelsen, L., Scholz, F., Hensen, C., Oschlies, A., & Wallmann, K. (2015). A revised global estimate of dissolved iron fluxes from marine sediments. Global Biogeochemical Cycles, 29(5), 691–707. https://doi.org/10.1002/2014gb005017
- Damien, P., Bianchi, D., McWilliams, J. C., Kessouri, F., Deutsch, C., Chen, R., & Renault, L. (2023). Enhanced biogeochemical cycling along the U.S. West Coast shelf. *Global Biogeochemical Cycles*, 37(1), e2022GB007572. https://doi.org/10.1029/2022GB007572
- Dauhajre, D. P., McWilliams, J. C., & Uchiyama, Y. (2017). Submesoscale coherent structures on the continental shelf. *Journal of Physical Oceanography*, 47(12), 2949–2976. https://doi.org/10.1175/jpo-d-16-0270.1
- Deutsch, C., Frenzel, H., McWilliams, J. C., Renault, L., Kessouri, F., Howard, E., et al. (2021). Biogeochemical variability in the California current system. *Progress in Oceanography*, 196, 102565. https://doi.org/10.1016/j.pocean.2021.102565
- Dinniman, M. S., St-Laurent, P., Arrigo, K. R., Hofmann, E. E., & van Dijken, G. L. (2020). Analysis of iron sources in Antarctic continental shelf
- waters. Journal of Geophysical Research: Oceans, 125(5), e2019JC015736. https://doi.org/10.1029/2019JC015736

 Duce, R. A., & Tindale, N. W. (1991). Atmospheric transport of iron and its deposition in the ocean. Limnology & Oceanography, 36(8),
- 1715–1726. https://doi.org/10.4319/lo.1991.36.8.1715
 Elrod, V. A., Berelson, W. M., Coale, K. H., & Johnson, K. S. (2004). The flux of iron from continental shelf sediments: A missing source for
- global budgets. Geophysical Research Letters, 31(12), L12307. https://doi.org/10.1029/2004GL020216
- Fennel, K., & Testa, J. M. (2019). Biogeochemical controls on coastal hypoxia. Annual Review of Marine Science, 11(1), 105–130. https://doi.org/10.1146/annurev-marine-010318-095138
- Fiechter, J., & Moore, A. M. (2012). Iron limitation impact on eddy-induced ecosystem variability in the coastal Gulf of Alaska. *Journal of Marine Systems*, 92(1), 1–15. https://doi.org/10.1016/j.jmarsys.2011.09.012
- Firme, G. F., Rue, E. L., Weeks, D. A., Bruland, K. W., & Hutchins, D. A. (2003). Spatial and temporal variability in phytoplankton iron limitation along the California coast and consequences for Si, N, and C biogeochemistry. *Global Biogeochemical Cycles*, 17(1). https://doi.org/10.1029/2001.02001824
- Fitzsimmons, J. N., Boyle, E. A., & Jenkins, W. J. (2014). Distal transport of dissolved hydrothermal iron in the deep South Pacific Ocean.

 Proceedings of the National Academy of Sciences of the United States of America, 111(47), 16654–16661. https://doi.org/10.1073/pnas.
 1418778111
- Frenger, I., Bianchi, D., Stührenberg, C., Oschlies, A., Dunne, J., Deutsch, C., et al. (2018). Biogeochemical role of subsurface coherent eddies in the ocean: Tracer cannonballs, hypoxic storms, and microbial stewpots? *Global Biogeochemical Cycles*, 32(2), 226–249. https://doi.org/10.1002/2017/GR005743
- Hawco, N. J., Barone, B., Church, M. J., Babcock-Adams, L., Repeta, D. J., Wear, E. K., et al. (2021). Iron depletion in the deep chlorophyll maximum: Mesoscale eddies as natural iron fertilization experiments. Global Biogeochemical Cycles, 35(12), e2021GB007112. https://doi.org/10.1029/2021GB007112
- Hogle, S. L., Dupont, C. L., Hopkinson, B. M., King, A. L., Buck, K. N., Roe, K. L., et al. (2018). Pervasive iron limitation at subsurface chlorophyll maxima of the California current. Proceedings of the National Academy of Sciences of the United States of America, 115(52), 13300–13305, https://doi.org/10.1073/pnas.1813192115
- Honeyman, B. D., Balistrieri, L. S., & Murray, J. W. (1988). Oceanic trace metal scavenging: The importance of particle concentration. *Deep-Sea Research, Part A: Oceanographic Research Papers*, 35(2), 227–246. https://doi.org/10.1016/0198-0149(88)90038-6
- Jersild, A., Delawalla, S., & Ito, T. (2021). Mesoscale eddies regulate seasonal iron supply and carbon drawdown in the Drake Passage. Geophysical Research Letters, 48(24), e2021GL096020. https://doi.org/10.1029/2021GL096020
- Jickells, T. D., An, Z. S., Andersen, K. K., Baker, A. R., Bergametti, G., Brooks, N., et al. (2005). Global iron connections between desert dust, ocean biogeochemistry, and climate. Science, 308(5718), 67–71. https://doi.org/10.1126/science.1105959
- John, S. G., Mendez, J., Moffett, J., & Adkins, J. (2012). The flux of iron and iron isotopes from San Pedro Basin sediments. Geochimica et Cosmochimica Acta, 93, 14–29. https://doi.org/10.1016/j.gca.2012.06.003
- Johnson, K. S., Chavez, F. P., & Friederich, G. E. (1999). Continental-shelf sediment as a primary source of iron for coastal phytoplankton. Nature, 398(6729), 697–700. https://doi.org/10.1038/19511
- Johnson, K. S., Elrod, V. A., Fitzwater, S. E., Plant, J. N., Chavez, F. P., Tanner, S. J., et al. (2003). Surface ocean-lower atmosphere interactions in the northeast Pacific Ocean gyre: Aerosols, iron, and the ecosystem response. Global Biogeochemical Cycles, 17(2). https://doi.org/10.1029/ 2002GB002004
- Keith Johnson, W., Miller, L. A., Sutherland, N. E., & Wong, C. (2005). Iron transport by mesoscale Haida eddies in the Gulf of Alaska. *Deep Sea Research Part II: Topical Studies in Oceanography*, 52(7), 933–953. https://doi.org/10.1016/j.dsr2.2004.08.017
- Kessouri, F., Bianchi, D., Renault, L., McWilliams, J. C., Frenzel, H., & Deutsch, C. A. (2020). Submesoscale currents modulate the seasonal cycle of nutrients and productivity in the California current system. Global Biogeochemical Cycles, 34(10), e2020GB006578. https://doi.org/10.1029/2020GB006578
- Kessouri, F., McWilliams, C. J., Deutsch, C., Renault, L., Frenzel, H., Bianchi, D., & Molemaker, J. (2022). ROMS-BEC oceanic physical and biogeochemical model code for the southern California current system version V2 [Model code]. Zenodo. https://doi.org/10.5281/zenodo. 6886319
- King, A. L., & Barbeau, K. (2007). Evidence for phytoplankton iron limitation in the southern California current system. Marine Ecology Progress Series, 342, 91–103. https://doi.org/10.3354/meps342091
- King, A. L., & Barbeau, K. A. (2011). Dissolved iron and macronutrient distributions in the southern California current system. *Journal of Geophysical Research*, 116(C3), C03018. https://doi.org/10.1029/2010JC006324
- Krachler, R., & Krachler, R. F. (2021). Northern high-latitude organic soils as a vital source of river-borne dissolved iron to the ocean. Environmental Science & Technology, 55(14), 9672–9690. https://doi.org/10.1021/acs.est.1c01439
- Kwiatkowski, L., Torres, O., Bopp, L., Aumont, O., Chamberlain, M., Christian, J. R., et al. (2020). Twenty-first century ocean warming, acidification, deoxygenation, and upper-ocean nutrient and primary production decline from CMIP6 model projections. *Biogeosciences*, 17(13), 3439–3470. https://doi.org/10.5194/bg-17-3439-2020

PHAM ET AL. 16 of 19



Global Biogeochemical Cycles

- 10.1029/2023GB008029
- Lam, P. J., Bishop, J. K. B., Henning, C. C., Marcus, M. A., Waychunas, G. A., & Fung, I. Y. (2006). Wintertime phytoplankton bloom in the subarctic Pacific supported by continental margin iron. *Global Biogeochemical Cycles*, 20(1). https://doi.org/10.1029/2005GB002557
- Lam, P. J., Heller, M. I., Lerner, P. E., Moffett, J. W., & Buck, K. N. (2020). Unexpected source and transport of iron from the deep Peru Margin. ACS Earth and Space Chemistry, 4(7), 977–992. https://doi.org/10.1021/acsearthspacechem.0c00066
- Laruelle, G. G., Dürr, H. H., Lauerwald, R., Hartmann, J., Slomp, C. P., Goossens, N., & Regnier, P. A. G. (2013). Global multi-scale segmentation of continental and coastal waters from the watersheds to the continental margins. *Hydrology and Earth System Sciences*, 17(5), 2029–2051. https://doi.org/10.5194/hess-17-2029-2013
- Lee, M.-M., & Coward, A. (2003). Eddy mass transport for the southern ocean in an eddy-permitting global ocean model. *Ocean Modelling*, 5(3), 249–266. https://doi.org/10.1016/S1463-5003(02)00044-6
- Liu, T., Krisch, S., Xie, R. C., Hopwood, M. J., Dengler, M., & Achterberg, E. P. (2022). Sediment release in the Benguela Upwelling System dominates trace metal input to the shelf and eastern South Atlantic Ocean. *Global Biogeochemical Cycles*, 36(9), e2022GB007466. https://doi. org/10.1029/2022GB007466
- Liu, X., & Millero, F. J. (2002). The solubility of iron in seawater. *Marine Chemistry*, 77(1), 43–54. https://doi.org/10.1016/S0304-4203(01)
- Lovecchio, E., Gruber, N., Münnich, M., & Frenger, I. (2022). On the processes sustaining biological production in the offshore propagating eddies of the northern canary upwelling system. *Journal of Geophysical Research: Oceans*, 127(2), e2021JC017691. https://doi.org/10.1029/2021JC017691
- Mahowald, N. M., Baker, A. R., Bergametti, G., Brooks, N., Duce, R. A., Jickells, T. D., et al. (2005). Atmospheric global dust cycle and iron inputs to the ocean. *Global Biogeochemical Cycles*, 19(4). https://doi.org/10.1029/2004GB002402
- McCoy, D., Bianchi, D., & Stewart, A. L. (2020). Global observations of submesoscale coherent vortices in the ocean. *Progress in Oceanography*, 189, 102452. https://doi.org/10.1016/j.pocean.2020.102452
- McWilliams, J. C. (1985). Submesoscale, coherent vortices in the ocean. Reviews of Geophysics, 23(2), 165–182. https://doi.org/10.1029/rg023i002p00165
- McWilliams, J. C. (2016). Submesoscale currents in the ocean. *Proceedings of the Royal Society A: Mathematical, Physical and Engineering Sciences*, 472(2189), 20160117. https://doi.org/10.1098/rspa.2016.0117
- Messié, M., & Chavez, F. P. (2015). Seasonal regulation of primary production in eastern boundary upwelling systems. *Progress in Oceanog-raphy*, 134, 1–18. https://doi.org/10.1016/j.pocean.2014.10.011
- Misumi, K., Nishioka, J., Obata, H., Tsumune, D., Tsubono, T., Long, M. C., et al. (2021). Slowly sinking particles underlie dissolved iron transport across the Pacific Ocean. *Global Biogeochemical Cycles*, 35(4), e2020GB006823. https://doi.org/10.1029/2020GB006823
- Moffett, J. W., & Boiteau, R. M. (2024). Metal organic complexation in seawater: Historical background and future directions. *Annual Review of*
- Marine Science, 16(1), 577–599. https://doi.org/10.1146/annurev-marine-033023-083652
 Molemaker, M. J., McWilliams, J. C., & Dewar, W. K. (2015). Submesoscale instability and generation of mesoscale anticyclones near a sep-
- aration of the California undercurrent. *Journal of Physical Oceanography*, 45(3), 613–629. https://doi.org/10.1175/jpo-d-13-0225.1 Moore, C. M., Mills, M. M., Arrigo, K. R., Berman-Frank, I., Bopp, L., Boyd, P. W., et al. (2013). Processes and patterns of oceanic nutrient
- limitation. Nature Geoscience, 6(9), 701–710. https://doi.org/10.1038/ngeo1765
- Moore, J. K., & Abbott, M. R. (2000). Phytoplankton chlorophyll distributions and primary production in the southern ocean. *Journal of Geophysical Research*, 105(C12), 28709–28722. https://doi.org/10.1029/1999JC000043
- Moore, J. K., & Braucher, O. (2008). Sedimentary and mineral dust sources of dissolved iron to the world ocean. *Biogeosciences*, 5(3), 631–656. https://doi.org/10.5194/bg-5-631-2008
- Moore, J. K., Doney, S. C., & Lindsay, K. (2004). Upper ocean ecosystem dynamics and iron cycling in a global three-dimensional model. *Global Biogeochemical Cycles*, 18(4). https://doi.org/10.1029/2004GB002220
- Pelland, N. A., Eriksen, C. C., & Lee, C. M. (2013). Subthermocline eddies over the Washington continental slope as observed by Seagliders, 2003–09. *Journal of Physical Oceanography*, 43(10), 2025–2053. https://doi.org/10.1175/jpo-d-12-086.1
- Person, R., Vancoppenolle, M., Aumont, O., & Malsang, M. (2021). Continental and sea ice iron sources fertilize the southern ocean in synergy. Geophysical Research Letters, 48(23), e2021GL094761. https://doi.org/10.1029/2021GL094761
- Pierce, S., Smith, R., Kosro, P., Barth, J., & Wilson, C. (2000). Continuity of the poleward undercurrent along the eastern boundary of the midlatitude North Pacific. *Deep Sea Research Part II: Topical Studies in Oceanography*, 47(5–6), 811–829. https://doi.org/10.1016/s0967-0645 (99)00128-9
- Rapp, I., Schlosser, C., Browning, T. J., Wolf, F., Le Moigne, F. A. C., Gledhill, M., & Achterberg, E. P. (2020). El Niño-driven oxygenation impacts Peruvian shelf iron supply to the South Pacific Ocean. *Geophysical Research Letters*, 47(7), e2019GL086631. https://doi.org/10.1029/ 2019GL086631
- Renault, L., McWilliams, J. C., Kessouri, F., Jousse, A., Frenzel, H., Chen, R., & Deutsch, C. (2021). Evaluation of high-resolution atmospheric and oceanic simulations of the California current system. *Progress in Oceanography*, 195, 102564. https://doi.org/10.1016/j.pocean.2021. 102564
- Resing, J. A., Sedwick, P. N., German, C. R., Jenkins, W. J., Moffett, J. W., Sohst, B. M., & Tagliabue, A. (2015). Basin-scale transport of hydrothermal dissolved metals across the South Pacific Ocean. *Nature*, 523(7559), 200–203. https://doi.org/10.1038/nature14577
- Richon, C., Aumont, O., & Tagliabue, A. (2020). Prey stoichiometry drives iron recycling by zooplankton in the global ocean. Frontiers in Marine Science, 7, 451. https://doi.org/10.3389/fmars.2020.00451
- Robinson, D., Pham, A. L., Yousavich, D. J., Janssen, F., Wenzhöfer, F., Arrington, E. C., et al. (2022). Iron "ore" nothing: Benthic iron fluxes from the oxygen-deficient Santa Barbara Basin enhance phytoplankton productivity in surface waters. *Biogeosciences Discussions*, 1–36.
- Scholz, F., Löscher, C. R., Fiskal, A., Sommer, S., Hensen, C., Lomnitz, U., et al. (2016). Nitrate-dependent iron oxidation limits iron transport in anoxic ocean regions. Earth and Planetary Science Letters, 454, 272–281. https://doi.org/10.1016/j.epsl.2016.09.025
- Severmann, S., McManus, J., Berelson, W. M., & Hammond, D. E. (2010). The continental shelf benthic iron flux and its isotope composition. Geochimica et Cosmochimica Acta, 74(14), 3984–4004. https://doi.org/10.1016/j.gca.2010.04.022
- Shchepetkin, A. F. (2015). An adaptive, courant-number-dependent implicit scheme for vertical advection in oceanic modeling. *Ocean Modelling*, 91, 38–69. https://doi.org/10.1016/j.ocemod.2015.03.006
- Shchepetkin, A. F., & McWilliams, J. C. (2005). The regional oceanic modeling system (ROMS): A split-explicit, free-surface, topography-following-coordinate oceanic model. *Ocean Modelling*, 9(4), 347–404. https://doi.org/10.1016/j.ocemod.2004.08.002
- Siedlecki, S. A., Mahadevan, A., & Archer, D. E. (2012). Mechanism for export of sediment-derived iron in an upwelling regime. *Geophysical Research Letters*, 39(3), L03601. https://doi.org/10.1029/2011GL050366

PHAM ET AL. 17 of 19

- St-Laurent, P., Yager, P. L., Sherrell, R. M., Oliver, H., Dinniman, M. S., & Stammerjohn, S. E. (2019). Modeling the seasonal cycle of iron and carbon fluxes in the Amundsen Sea Polynya, Antarctica. *Journal of Geophysical Research: Oceans*, 124(3), 1544–1565. https://doi.org/10.1029/2018JC014773
- St-Laurent, P., Yager, P. L., Sherrell, R. M., Stammerjohn, S. E., & Dinniman, M. S. (2017). Pathways and supply of dissolved iron in the Amundsen Sea (Antarctica). *Journal of Geophysical Research: Oceans*, 122(9), 7135–7162. https://doi.org/10.1002/2017JC013162
- Tagliabue, A., Aumont, O., DeAth, R., Dunne, J. P., Dutkiewicz, S., Galbraith, E., et al. (2016). How well do global ocean biogeochemistry models simulate dissolved iron distributions? Global Biogeochemical Cycles, 30(2), 149–174. https://doi.org/10.1002/2015GB005289
- Tagliabue, A., Barrier, N., Du Pontavice, H., Kwiatkowski, L., Aumont, O., Bopp, L., et al. (2020). An iron cycle cascade governs the response of equatorial Pacific ecosystems to climate change. *Global Change Biology*, 26(11), 6168–6179. https://doi.org/10.1111/gcb.15316
- Tagliabue, A., Bopp, L., Dutay, J.-C., Bowie, A. R., Chever, F., Jean-Baptiste, P., et al. (2010). Hydrothermal contribution to the oceanic dissolved iron inventory. *Nature Geoscience*, 3(4), 252–256. https://doi.org/10.1038/ngeo818
- Tagliabue, A., Bowie, A. R., Boyd, P. W., Buck, K. N., Johnson, K. S., & Saito, M. A. (2017). The integral role of iron in ocean biogeochemistry. Nature, 543(7643), 51–59. https://doi.org/10.1038/nature21058
- Tagliabue, A., Bowie, A. R., DeVries, T., Ellwood, M. J., Landing, W. M., Milne, A., et al. (2019). The interplay between regeneration and scavenging fluxes drives ocean iron cycling. *Nature Communications*, 10(1), 4960. https://doi.org/10.1038/s41467-019-12775-5
- Tagliabue, A., Sallee, J.-B., Bowie, A. R., Levy, M., Swart, S., & Boyd, P. W. (2014). Surface-water iron supplies in the southern ocean sustained by deep winter mixing. Natura Geography, 344, 320, https://doi.org/10.1038/ngeo.2101
- by deep winter mixing. Nature Geoscience, 7(4), 314–320. https://doi.org/10.1038/ngeo2101
 Tagliabue, A., Williams, R. G., Rogan, N., Achterberg, E. P., & Boyd, P. W. (2014). A ventilation-based framework to explain the regeneration-
- scavenging balance of iron in the ocean. *Geophysical Research Letters*, 41(20), 7227–7236. https://doi.org/10.1002/2014GL061066

 Thomson, R. E., & Krassovski, M. V. (2010). Poleward reach of the California undercurrent extension. *Journal of Geophysical Research*,
- 116(C9), C09027. https://doi.org/10.1029/2010JC006280
- Till, C. P., Solomon, J. R., Cohen, N. R., Lampe, R. H., Marchetti, A., Coale, T. H., & Bruland, K. W. (2019). The iron limitation mosaic in the California current system: Factors governing Fe availability in the shelf/near-shelf region. *Limnology & Oceanography*, 64(1), 109–123. https://doi.org/10.1002/lno.11022
- Uchida, T., Balwada, D., Abernathey, R. P., McKinley, G. A., Smith, S. K., & Lévy, M. (2020). Vertical eddy iron fluxes support primary production in the open southern ocean. *Nature Communications*, 11(1), 1125. https://doi.org/10.1038/s41467-020-14955-0
- van den Berg, C. M. G. (1995). Evidence for organic complexation of iron in seawater. *Marine Chemistry*, 50(1), 139–157. https://doi.org/10.1016/0304-4203(95)00032-M
- Vieira, L. H., Krisch, S., Hopwood, M. J., Beck, A. J., Scholten, J., Liebetrau, V., & Achterberg, E. P. (2020). Unprecedented Fe delivery from the Congo River margin to the South Atlantic Gyre. *Nature Communications*, 11(1), 556. https://doi.org/10.1038/s41467-019-14255-2
- Wallmann, K., José, Y. S., Hopwood, M. J., Somes, C. J., Dale, A. W., Scholz, F., et al. (2022). Biogeochemical feedbacks may amplify ongoing and future ocean deoxygenation: A case study from the Peruvian oxygen minimum zone. *Biogeochemistry*, 159(1), 45–67. https://doi.org/10.1007/s10533-022-00908-w
- Wanninkhof, R. (1992). Relationship between wind speed and gas exchange over the ocean. *Journal of Geophysical Research*, 97(C5), 7373–7382. https://doi.org/10.1029/92JC00188
- Weber, T., John, S., Tagliabue, A., & DeVries, T. (2018). Biological uptake and reversible scavenging of zinc in the global ocean. *Science*, 361(6397), 72–76. https://doi.org/10.1126/science.aap8532
- Wetz, M. S., Hales, B., Chase, Z., Wheeler, P. A., & Whitney, M. M. (2006). Riverine input of macronutrients, iron, and organic matter to the coastal ocean off Oregon, U.S.A., during the winter. *Limnology & Oceanography*, 51(5), 2221–2231. https://doi.org/10.4319/lo.2006.51.5.
- Wong, K. H., Nishioka, J., Kim, T., & Obata, H. (2022). Long-range lateral transport of dissolved manganese and iron in the subarctic Pacific. Journal of Geophysical Research: Oceans, 127(2), e2021JC017652. https://doi.org/10.1029/2021JC017652

References From the Supporting Information

- Abdala, Z. M., Clayton, S., Einarsson, S. V., Powell, K., Till, C. P., Coale, T. H., & Chappell, P. D. (2022). Examining ecological succession of diatoms in California current system cyclonic mesoscale eddies. *Limnology & Oceanography*, 67(11), 2586–2602. https://doi.org/10.1002/lno.
- Bundy, R. M., Barbeau, K. A., Carter, M., & Jiang, M. (2016). Iron-binding ligands in the southern California current system: Mechanistic studies. Frontiers in Marine Science, 3. https://doi.org/10.3389/fmars.2016.00027
- Elrod, V. A., Johnson, K. S., Fitzwater, S. E., & Plant, J. N. (2008). A long-term, high-resolution record of surface water iron concentrations in the upwelling-driven central California region. *Journal of Geophysical Research*, 113(C11), C11021. https://doi.org/10.1029/2007JC004610
- Feely, R. A., Alin, S. R., Carter, B., Bednaršek, N., Hales, B., Chan, F., et al. (2016). Chemical and biological impacts of ocean acidification along the west coast of North America. *Estuarine, Coastal and Shelf Science*, 183, 260–270. https://doi.org/10.1016/j.ecss.2016.08.043
- Fitzwater, S. E., Johnson, K. S., Elrod, V. A., Ryan, J. P., Coletti, L. J., Tanner, S. J., et al. (2003). Iron, nutrient and phytoplankton biomass relationships in upwelled waters of the California coastal system. *Continental Shelf Research*, 23(16), 1523–1544. https://doi.org/10.1016/j.csr. 2003.08.004
- Garcia, H., Locarnini, R., Boyer, T., Antonov, J., Baranova, O., Zweng, M., & Johnson, D. (2009). Dissolved oxygen, apparent oxygen utilization, and oxygen saturation. World Ocean Atlas, 3.
- Johnson, K. S., Chavez, F. P., Elrod, V. A., Fitzwater, S. E., Pennington, J. T., Buck, K. R., & Walz, P. M. (2001). The annual cycle of iron and the biological response in central California coastal waters. *Geophysical Research Letters*, 28(7), 1247–1250. https://doi.org/10.1029/ 2000GL012433
- Kelly, R. L., Bian, X., Feakins, S. J., Fornace, K. L., Gunderson, T., Hawco, N. J., et al. (2021). Delivery of metals and dissolved black carbon to the southern California coastal ocean via aerosols and floodwaters following the 2017 Thomas Fire. *Journal of Geophysical Research: Biogeosciences*, 126(3), e2020JG006117. https://doi.org/10.1029/2020JG006117
- Landing, W. M., & Bruland, K. W. (1987). The contrasting biogeochemistry of iron and manganese in the Pacific Ocean. Geochimica et Cosmochimica Acta, 51(1), 29–43. https://doi.org/10.1016/0016-7037(87)90004-4
- Lohan, M. C., & Bruland, K. W. (2008). Elevated Fe(ii) and dissolved Fe in hypoxic shelf waters off Oregon and Washington: An enhanced source of iron to coastal upwelling regimes. *Environmental Science & Technology*, 42(17), 6462–6468. https://doi.org/10.1021/es800144j

PHAM ET AL. 18 of 19



Global Biogeochemical Cycles

10.1029/2023GB008029

Martin, J. H., & Michael Gordon, R. (1988). Northeast Pacific iron distributions in relation to phytoplankton productivity. *Deep-Sea Research, Part A: Oceanographic Research Papers*, 35(2), 177–196. https://doi.org/10.1016/0198-0149(88)90035-0

Risien, C. M., Cervantes, B. T., Fewings, M. R., Barth, J. A., & Kosro, P. M. (2023). A stitch in time: Combining more than two decades of mooring data from the central Oregon shelf. *Data in Brief*, 48, 109041. https://doi.org/10.1016/j.dib.2023.109041

PHAM ET AL. 19 of 19